Topological Disclination States and Charge Fractionalization in a Non-Hermitian Lattice

Rimi Banerjee,[1] Subhaskar Mandal,[1] Yun Yong Terh,[1] Shuxin Lin,[1] Gui-Geng Liu,[1]
Baile Zhang,[1,2,*] and Y. D. Chong[1,2,†]

[1]*School of Physical and Mathematical Sciences, Nanyang Technological University, Singapore 637371, Singapore*
[2]*Centre for Disruptive Photonic Technologies, Nanyang Technological University, Singapore, 637371, Singapore*

(Received 5 June 2024; revised 21 September 2024; accepted 4 November 2024; published 5 December 2024)

We show that a non-Hermitian lattice with a disclination can host topological disclination states that are induced by on-site gain and loss. The disclination states are inherently non-Hermitian as they do not exist in the limit of zero gain or loss. They arise from charge fractionalization in the non-Hermitian lattice, which we establish using non-Hermitian Wilson loops calculated with biorthogonal products. The model is suitable for realization on established experimental platforms, such as arrays of photonic or polaritonic resonators. The emergence of the topological disclination states can manifest as an abrupt shift in emission intensity and frequency with varying gain or loss.

DOI: 10.1103/PhysRevLett.133.233804

Introduction—In discrete lattices, dislocations and disclinations are elementary defects that cannot be removed by local deformations due to their global topological structure [1–6]. They play an important role in many condensed-matter phenomena, such as the melting of two-dimensional solids [6]. In topological materials [7], such defects have a special significance: they obey "bulk-defect correspondences" that generalize the bulk-boundary correspondences that are the usual signatures for bulk band topology [8–24]. In certain higher-order topological insulators (HOTIs) [25–35], bulk-defect correspondences may be used to probe topological properties that are hard to access through boundary measurements [15,16]. Aside from the appearance of localized defect states, some bulk-defect correspondences predict charge fractionalization, whereby a fraction of a unit charge polarization is localized at the defect. This phenomenon results from an incompatibility between charge quantization and lattice symmetries (a filling anomaly), which underpins the topology of HOTIs [25–27]. Recently, charge fractionalization and localized states have been observed experimentally in 2D photonic lattices with disclinations [15,16].

Theoretical analyses of topological materials, including most earlier studies of bulk-defect correspondences, usually take Hermiticity as a starting assumption. In recent years, however, there has been increasing interest in non-Hermitian (NH) [36–38] topological materials [39–48]. Not only do such systems pose the theoretically interesting challenge of formulating band topology without Hermiticity, but they are also of practical interest: in the classical-wave metamaterials commonly used to realize topological phases, loss and gain are often non-negligible [49–55]. For example, topological lasers, which are promising technological applications of topological states, are inherently NH [56–61]. Research into NH band topology has uncovered numerous surprises, such as NH topological phases distinct from any Hermitian counterpart [39,40,48,62–64]. Other recent studies have shown that gain and loss can induce boundary states in 1D lattices [65–68] and corner states in 2D lattices [69,70]. To our knowledge, however, topological bulk-defect correspondences have not yet been studied in the NH regime.

In this Letter, we demonstrate that a NH lattice containing a disclination can host topological disclination states associated with fractional $(1/2)$ charge. Unlike the previously studied disclination states of Hermitian lattices [8–12,14–24], these NH disclination states are induced solely by on-site gain and loss, and are nonexistent in the Hermitian limit. The model consists of a 2D graphenelike honeycomb lattice with a disclination; the application of a specific pattern of gain or loss (imaginary on-site mass terms) generates a bulk gap in the real part of the energy spectrum, in which the disclination states appear [71–74]. Previously, gain- or loss-induced topological states have been found in NH models like the Takata-Notomi model, a 1D lattice hosting NH midgap boundary states [65], as well as a NH 2D HOTI with gain- or loss-induced corner states [69]. NH topological disclination states, however, have not yet been identified. (There have been some studies of how lattice defects affect the non-Hermitian skin effect, which is a separate issue [75–78].) Our work also establishes NH charge fractionalization at a lattice defect, a phenomenon previously limited to Hermitian models [14–16]. The charge fractionalization is established using Wilson loops derived from biorthogonal products, and also using a NH formulation of the density of states. We will also discuss an alternative model featuring NH disclination states unaccompanied by fractional charge.

*Contact author: blzhang@ntu.edu.sg
†Contact author: yidong@ntu.edu.sg

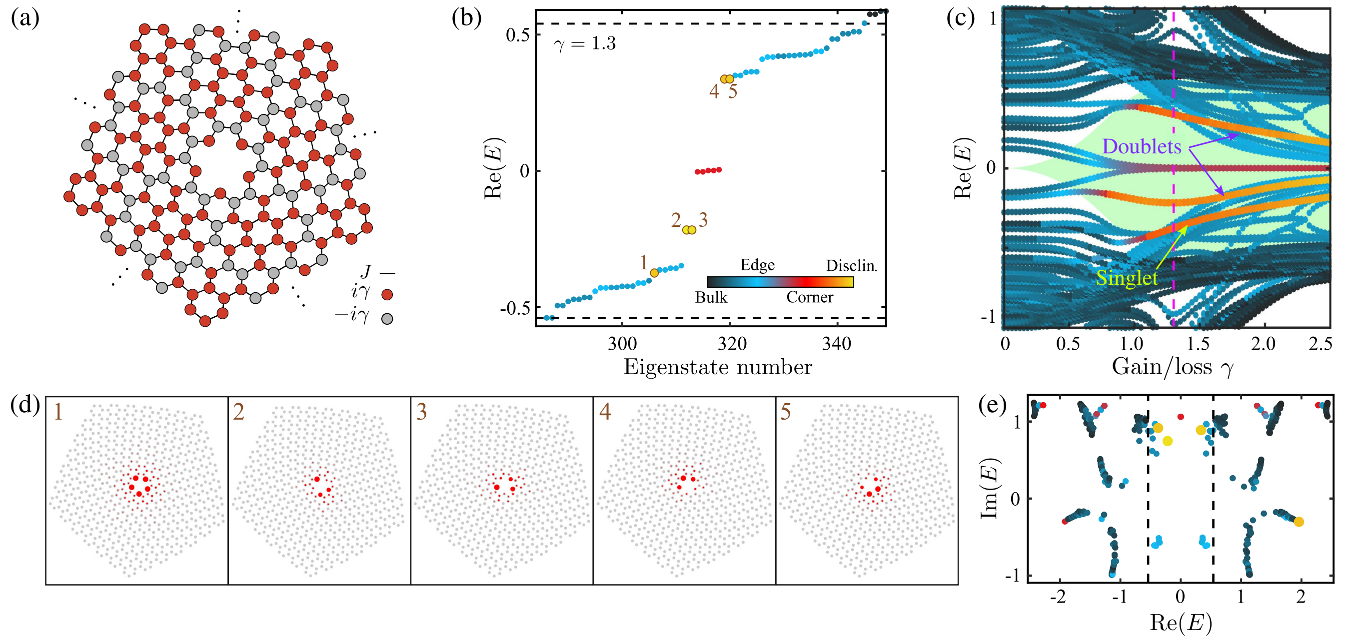

FIG. 1. (a) Schematic of a 2D NH lattice containing a disclination, with nearest-neighbor hopping J (black links) and on-site gain $i\gamma$ (red circles) or loss $-i\gamma$ (gray circles). (b) $\mathrm{Re}(E)$ spectrum for a 630-site lattice based on (a). Marker colors indicate the degree of localization to the bulk, edge, corners, and disclination (see Supplemental Material [79]). Horizontal dashes indicate the bulk gap obtained from Fig. 2(a), in which lie the edge, corner, and disclination states. The energies labeled 1–5 correspond to disclination states. (c) Plot of $\mathrm{Re}(E)$ versus γ, with the same marker color scheme as in (b). The shaded green area corresponds to the bulk gap, and vertical magenta dashes indicate the reference gain or loss level $\gamma = 1.3$. The range $\gamma < 0$ is omitted as it just gives the conjugate of the $\gamma > 0$ spectrum. (d) Intensity ($|\psi_n|^2$) distributions for the disclination states in (b). (e) Complex energy spectrum for the disclination-bearing lattice of (b) and (d). In all subplots, the hopping is $J = 1$.

Finally, we study the prospects for realizing such a NH lattice using pumped optical resonators. In this setting, the gain- or loss-induced topological disclination mode has a distinctive experimental signature in the form of an increase in emission intensity and abrupt shift in peak frequency as the gain or loss level is tuned. The unique properties of NH topological disclination states, which are gain- or loss-induced and yet possess a level of robustness due to their topological origins, may eventually be useful for designing novel lasers and related devices.

Model—We consider the 2D NH lattice shown in Fig. 1(a). The lattice structure is generated by introducing a disclination into a pristine honeycomb lattice, as explained below, with each nearest-neighbor pair of sites connected by a real hopping J. Each site contains gains (red circles) or losses (gray circles), which are represented by imaginary on-site mass terms $\pm i\gamma$, where $\gamma \geq 0$ is the gain or loss level [36]. The Hamiltonian is

$$H = \sum_n i\gamma_n a_n^\dagger a_n + J\sum_{\langle nn'\rangle}\left(a_{n'}^\dagger a_n + \mathrm{H.c.}\right), \qquad (1)$$

where $\gamma_n = \pm\gamma$, $a_n^\dagger$ and a_n are the creation and annihilation operators on site n, and $\langle nn'\rangle$ denotes nearest neighbors. For $\gamma = 0$, this reduces to a Hermitian graphene-type lattice with a disclination [10], which is known to have no bulk gap and no edge, corner, or disclination states [79].

For nonzero γ, Fig. 1(b) shows the real part of the spectrum. The lattice is based on Fig. 1(a) but expanded to 630 sites, with $\gamma = 1.3$ and $J = 1$. There are several eigenenergies near the center of the gap, marked in blue and red, which are edge and corner states localized to the outer boundary of the sample [79].

We also see five eigenenergies, two doublets and a singlet, marked in yellow. These turn out to be gain- or loss-induced disclination states. As shown in Fig. 1(c), they emerge into the bulk gap at nonzero values of γ. Their intensity distributions (i.e., $|\psi_n|^2$, where ψ_n is an energy eigenfunction on site n) are localized to the disclination core, as shown in Fig. 1(d). Figure 1(e) shows where the eigenenergies are located in the complex E plane.

To understand these results, consider the related disclination-free NH honeycomb lattice shown in Fig. 2(a). It has C_6 rotational symmetry, with a unit cell (yellow hexagon) of 18 sites. The lattice of Fig. 1(a) can be generated from this through a Volterra ("cut-and-glue") process, by removing a $\pi/3$ sector (blue-shaded region) and reconnecting the seams. With the chosen gain or loss distribution, there is no seam or discontinuity after the Volterra process. Other gain or loss distributions, despite being simpler, lack this crucial property.

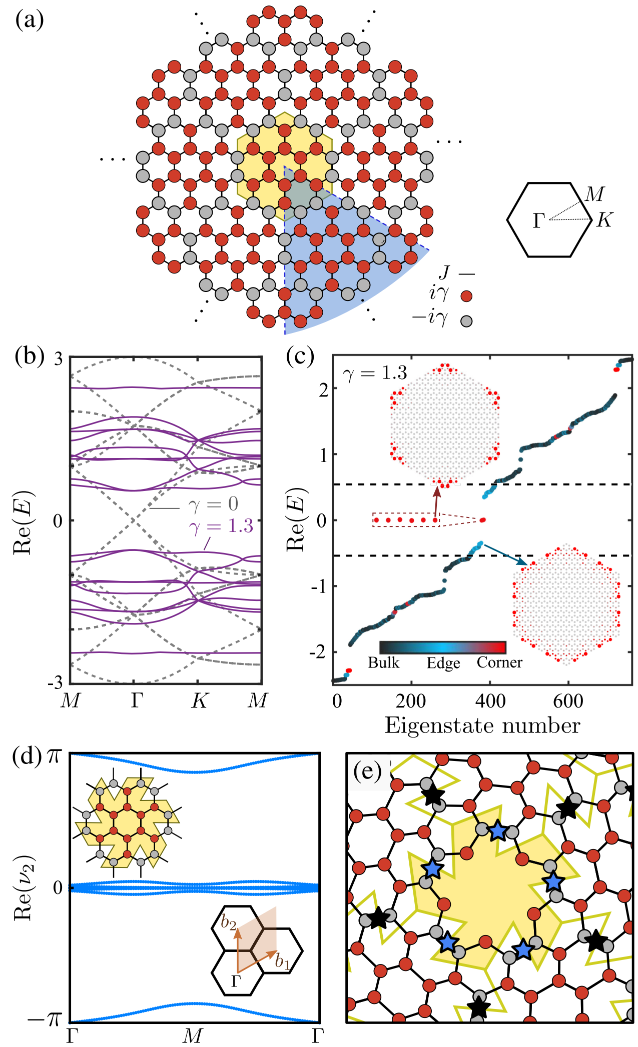

FIG. 2. (a) Schematic of a 2D NH honeycomb lattice with an 18-site unit cell (yellow region). From this, Fig. 1(a) can be generated by cutting out a $\pi/3$ sector (blue region). (b) Real bulk band diagram for $\gamma = 0$ (gray dashes) and $\gamma = 1.3$ (purple lines). (c) $\mathrm{Re}(E)$ spectrum for a 762-site hexagonal sample with $\gamma = 1.3$. Marker colors indicate the degree of localization to the bulk, edge, and corners [79]. In the bulk gap (horizontal dashes), there are edge and corner states, with the latter pinned to $\mathrm{Re}(E) = 0$. Inset: intensity ($|\psi|^2$) distributions for representative corner and edge states. (d) Wilson loops for the lowest nine bands at $\gamma = 1.3$. Upper inset: the unit cell for this calculation [79]. Lower inset: layout of Brillouin zones and reciprocal lattice vectors $b_{1,2}$. (e) Positions of Wannier centers (black and blue stars) near the disclination. Those adjacent to the disclination core (blue stars) yield a fractional charge of 1/2 (mod 1). In all subplots, $J = 1$.

Figure 2(b) shows the real part of the bulk band diagram for the NH lattice of Fig. 2(a), with hopping $J = 1$. In the Hermitian limit (i.e., $\gamma = 0$), the eigenenergies are real and gapless (gray dashes); this is simply the band diagram for graphene, with the original K and K' points folded onto Γ. For $\gamma \neq 0$, a real line gap—i.e., a gap in the real part of the energy, $\mathrm{Re}(E)$ [48]—opens up around $\mathrm{Re}(E) = 0$ (purple lines). In Fig. 2(c), we plot $\mathrm{Re}(E)$ for a finite hexagonal sample with 762 sites. This spectrum exhibits the same real line gap as the bulk system, but with additional edge and corner states occupying the bulk gap. The intensity distributions for two exemplary states are plotted in the inset of Fig. 2(c). (There are also trivial corner states lying outside the gap [79].) Evidently, the lattice behaves much like a NH version of a HOTI [25], with the nonzero gain and loss generating a real line gap as well as in-gap boundary states [69,79].

Topological characterization—In Hermitian HOTIs, the topological states are tied to the deeper phenomenon of robust charge fractionalization [14–16]. Here, we argue that the disclination in the present NH model induces a fractional charge of 1/2.

For the periodic lattice of Fig. 2(a), we numerically calculate Wilson loops involving all nine bands situated below the real line gap. We first adjust the shape of the unit cell to avoid the ambiguity of certain sites falling on the edges of the unit cell [Fig. 2(d), upper inset]. Next, the first Brillouin zone is discretized along the reciprocal lattice vectors b_1 and b_2 [Fig. 2(d), lower inset]. Starting from a given k, the Wilson loop matrices are [69,70]

$$W_j = F_j(k + N\Delta k_j) \cdots F_j(k + \Delta k_j) F_j(k), \qquad (2)$$

where N is the number of discretization points in the b_j direction, Δk_j is the wave vector step, and $F_j(k)$ is a 9×9 matrix of biorthogonal products,

$$F_j^{mn}(k) = \langle u_m^L(k + \Delta k_j) | u_n^R(k) \rangle. \qquad (3)$$

Here, m, n index bands below the line gap at $\mathrm{Re}(E) = 0$, and $u^{L/R}(k)$ denotes left and right eigenvectors of the Bloch Hamiltonian, which satisfy the biorthogonality relation $\langle u_m^L(k) | u_n^R(k) \rangle = \delta_{mn}$ [36].

From the eigenvalues λ_j of W_j, we retrieve the phases $\nu_j = -i \ln(\lambda_j)$. Figure 2(d) plots $\mathrm{Re}(\nu_2)$ as the initial k point varies along the b_1 direction. Throughout this trajectory, $\mathrm{Im}(\nu_2)$ is close to zero. The plot for $\mathrm{Re}(\nu_1)$, as k varies along b_2, behaves very similarly and is thus omitted. The Wilson loop exhibits no overall winding, but crosses $\pm\pi$ an odd number of times. This is the same behavior found in the Hermitian Wu-Hu model, using standard inner products for the W_j matrices [88–91]. That Hermitian model is known to belong to the 2D Stiefel-Whitney class and supports a HOTI phase with Wannier centers at the $3c$ Wyckoff position [91–93].

Informed by these results, we take a close-up view of the disclination-bearing lattice from Fig. 1(a). As shown in Fig. 2(e), the Wannier centers (black and blue stars) lie at the boundaries of the unit cells, contributing 1/2 (mod 1) spectral charge to each adjacent cell [14,15]. Since the boundary of the disclination core crosses an odd number of Wannier centers (blue stars), the disclination carries a fractional charge of 1/2 (mod 1). In Hermitian lattices, a similar argument for charge fractionalization at disclinations [14] has been verified in experiments on microwave metamaterials and photonic crystals [15,16].

Another way to identify disclination charge is to examine the local density of states [15,16,27]. For each site j, we define the expected density

$$\langle \Pi_{jm} \rangle = \langle \psi_m^L | \Pi_j | \psi_m^R \rangle, \tag{4}$$

where $\Pi_j = |j\rangle\langle j|$ is a local projection operator and $|\psi_m^{L/R}\rangle$ are the biorthogonal mth left and right eigenstates of the full lattice. For our NH model, $\langle \Pi_{jm} \rangle$ is complex-valued [48,94,95]. We define the disclination charge as

$$Q_d = \sum_{mj} |\langle \Pi_{jm} \rangle| (\mathrm{mod}\ 1), \tag{5}$$

with j summed over sites near the disclination core [79], and m summed over all states below the bulk gap—i.e., Re(E) below the bottom dashes in Fig. 1(b). For the lattice of Fig. 2(e), we obtain $Q_d = 0.53$, close to the predicted value of 0.5.

Alternative gain or loss pattern—Figures 3(a),(b) show a lattice with an alternative gain or loss distribution. Like the previous design, the periodic lattice has 18 sites per unit cell, and the gain or loss pattern produces no seam under the Volterra process. For $\gamma \neq 0$, this lattice exhibits a real line gap, but no corner or disclination states (for details, see the Supplemental Material [79]). We thus interpret this as a NH analog of a HOTI in the trivial phase. Moreover, if we apply a disclination with a Frank angle of $2\pi/3$, the resulting C_4-symmetric lattice *does* host a midgap disclination state [79], consistent with Deng *et al.*'s finding that a Wu-Hu lattice in its trivial phase hosts a disclination state for a $2\pi/3$ disclination but not a $\pi/3$ disclination [21].

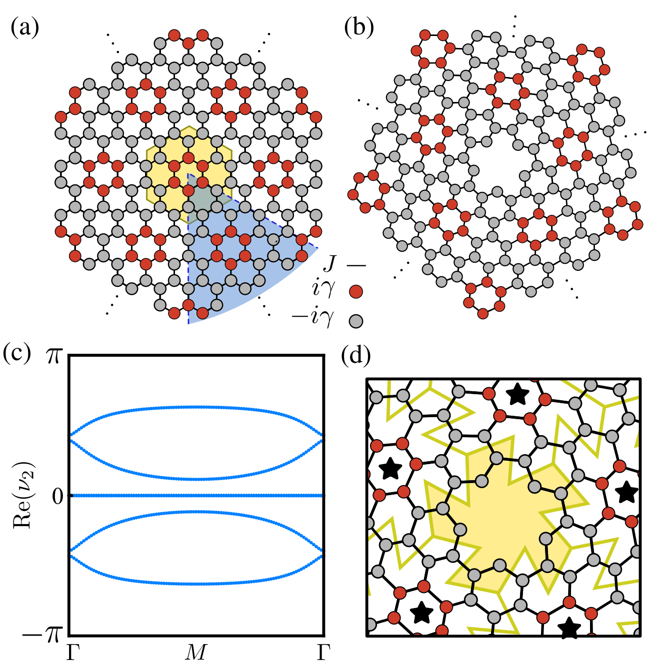

FIG. 3. (a),(b) An alternative NH lattice, similar to Figs. 1(a) and 2(a), but with a different gain or loss pattern. (c) Wilson loop for the lowest nine bands, with $J = 1$ and $\gamma = 0.75$. (d) Close-up view of the disclination-bearing lattice, with the Wannier centers marked by black stars.

Repeating the Wilson loop calculation for this case, we obtain the results shown in Fig. 3(c), consisting of trivial windings reminiscent of the trivial phase of the Hermitian Wu-Hu model with Wannier centers at the $1a$ Wyckoff position [92,93]. Figure 3(d) shows the positions of the Wannier centers (black stars), which lie at the centers of the unit cells and thus do not contribute fractional charge to the disclination core. This is consistent with the lattice's aforementioned lack of gain- or loss-induced disclination-bound states, and further supported by the charge calculation yielding $Q_d = -0.08$.

Experimental signatures—The present model should be realizable using established experimental platforms, such as photonic lattices [66,67,70,96–98]. The model's intersite hoppings are reciprocal, positive, and nearest-neighbor, with the non-Hermiticity entering only in the form of onsite gain and loss. A likely complication in real lattices is that the intersite hoppings may be spatially inhomogeneous due to varying distances between resonators, but our numerical studies indicate that this does not substantially alter the disclination states [79].

As an example of how the NH disclination states could be identified in an experiment, we insert the lattice of Fig. 1(a) into a driven Schrödinger equation,

$$i\frac{\partial \psi}{\partial t} = H\psi - i\gamma\psi + Fe^{-i\omega_0 t}, \tag{6}$$

where ψ is the state vector, H is the NH lattice Hamiltonian, and an additional loss γ is applied to all sites. This can describe a setup where individual sites have fixed loss and tunable gain, such that one sublattice has zero net gain and loss and the other has loss 2γ. We also include an excitation of frequency ω_0 and spatially dependent amplitude F. Exploiting the phase profiles of the disclination states [79], we concentrate F on three disclination core sites, indicated in the inset of Fig. 4(a), to create a strong overlap with a specific disclination state. Figure 4(a) shows the resulting intensity spectrum on the five disclination core sites. With increasing γ, the intensity peak shifts closer to midgap and grows greatly in magnitude. As shown in Fig. 4(b), the peak frequency jumps abruptly, coinciding with the emergence of the disclination state into the gain- or loss-induced bulk gap. The steady-state intensity profiles, plotted in Fig. 4(c), show strong localization in the large-γ regime. Note that Eq. (6) is also very close to the model equations for a polaritonic lattice [56,60,68,80–84,99–101], except for the omission of nonlinearities [85]. In the Supplemental

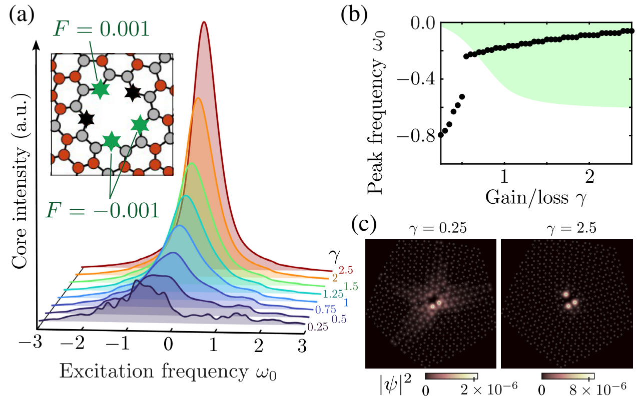

FIG. 4. (a) Time domain simulation results for a disclination-bearing lattice [Fig. 1(a)] driven by a monochromatic excitation on three sites at the disclination core (green stars, inset), with $F = 0$ on all other sites. The intensity on the core sites ($\sum_n |\psi_n|^2$, summing over on the five starred sites in the inset) is plotted against the excitation frequency ω_0 for different γ, with $J = 1$. (b) Plot of peak frequency versus γ. The shaded green area indicates the bulk gap of the undriven lattice. (c) Steady-state intensity profile for two values of γ. For large γ, the intensity is strongly localized to the disclination core.

Material, we investigate the role of such nonlinearities and find that they can cause the disinclination states to exhibit bistability [79].

Conclusion—We have shown that disclinations in 2D lattices can host non-Hermitian disclination states, which emerge when a bulk gap is created by a specific pattern of gain or loss on the lattice sites. The disclinations carry fractional charge 1/2, thereby extending recent results on Hermitian topological disclination states into the non-Hermitian case. Because these topological disclination states are induced by gain or loss tuning, they might be used as the basis for novel lasers whose modes can be manipulated via selective pumping.

Acknowledgments—This work was supported by the National Research Foundation (NRF), Singapore under Competitive Research Programme NRF-CRP23-2019-0005 and NRF-CRP23-2019-0007, and NRF Investigatorship NRF-NRFI08-2022-0001, and by Singapore Ministry of Education Academic Research Tier 2 grant (MOE-T2EP50123-0007) and Tier 1 grant (RG139/22).

Data availability—The Hamiltonian matrices for the finite 2D lattices used in this study are available in the Nanyang Technological University data repository [102].

[1] N. D. Mermin, The topological theory of defects in ordered media, Rev. Mod. Phys. **51**, 591 (1979).
[2] M. T. Lusk and L. D. Carr, Nanoengineering defect structures on graphene, Phys. Rev. Lett. **100**, 175503 (2008).
[3] K. S. Kim, Y. Zhao, H. Jang, S. Y. Lee, J. M. Kim, K. S. Kim, J.-H. Ahn, P. Kim, J.-Y. Choi, and B. H. Hong, Large-scale pattern growth of graphene films for stretchable transparent electrodes, Nature (London) **457**, 706 (2009).
[4] Y. Wei, J. Wu, H. Yin, X. Shi, R. Yang, and M. Dresselhaus, The nature of strength enhancement and weakening by pentagon–heptagon defects in graphene, Nat. Mater. **11**, 759 (2012).
[5] J. Wu and Y. Wei, Grain misorientation and grain-boundary rotation dependent mechanical properties in polycrystalline graphene, J. Mech. Phys. Solids **61**, 1421 (2013).
[6] J. M. Kosterlitz, Nobel lecture: Topological defects and phase transitions, Rev. Mod. Phys. **89**, 040501 (2017).
[7] M. Z. Hasan and C. L. Kane, Colloquium: Topological insulators, Rev. Mod. Phys. **82**, 3045 (2010).
[8] Y. Ran, Y. Zhang, and A. Vishwanath, One-dimensional topologically protected modes in topological insulators with lattice dislocations, Nat. Phys. **5**, 298 (2009).
[9] J. C. Y. Teo and T. L. Hughes, Existence of majorana-fermion bound states on disclinations and the classification of topological crystalline superconductors in two dimensions, Phys. Rev. Lett. **111**, 047006 (2013).
[10] A. Rüegg and C. Lin, Bound states of conical singularities in graphene-based topological insulators, Phys. Rev. Lett. **110**, 046401 (2013).
[11] W. A. Benalcazar, J. C. Y. Teo, and T. L. Hughes, Classification of two-dimensional topological crystalline superconductors and Majorana bound states at disclinations, Phys. Rev. B **89**, 224503 (2014).
[12] F.-F. Li, H.-X. Wang, Z. Xiong, Q. Lou, P. Chen, R.-X. Wu, Y. Poo, J.-H. Jiang, and S. John, Topological light-trapping on a dislocation, Nat. Commun. **9**, 2462 (2018).
[13] J. C. Y. Teo and C. L. Kane, Topological defects and gapless modes in insulators and superconductors, Phys. Rev. B **82**, 115120 (2010).
[14] T. Li, P. Zhu, W. A. Benalcazar, and T. L. Hughes, Fractional disclination charge in two-dimensional C_n-symmetric topological crystalline insulators, Phys. Rev. B **101**, 115115 (2020).
[15] Y. Liu, S. Leung, F.-F. Li, Z.-K. Lin, X. Tao, Y. Poo, and J.-H. Jiang, Bulk-disclination correspondence in topological crystalline insulators, Nature (London) **589**, 381 (2021).
[16] C. W. Peterson, T. Li, W. Jiang, T. L. Hughes, and G. Bahl, Trapped fractional charges at bulk defects in topological insulators, Nature (London) **589**, 376 (2021).
[17] Q. Wang, H. Xue, B. Zhang, and Y. D. Chong, Observation of protected photonic edge states induced by real-space topological lattice defects, Phys. Rev. Lett. **124**, 243602 (2020).
[18] Q. Wang, Y. Ge, H. xiang Sun, H. Xue, D. Jia, Y. jun Guan, S. qi Yuan, B. Zhang, and Y. D. Chong, Vortex states in an acoustic Weyl crystal with a topological lattice defect, Nat. Commun. **12**, 3654 (2021).
[19] H. Xue, D. Jia, Y. Ge, Y. J. Guan, Q. Wang, S. Q. Yuan, H. X. Sun, Y. D. Chong, and B. Zhang, Observation of dislocation-induced topological modes in a three-dimensional acoustic topological insulator, Phys. Rev. Lett. **127**, 214301 (2021).

[20] M. Geier, I. C. Fulga, and A. Lau, Bulk-boundary-defect correspondence at disclinations in rotation-symmetric topological insulators and superconductors, SciPost Phys. **10**, 092 (2021).
[21] Y. Deng, W. A. Benalcazar, Z.-G. Chen, M. Oudich, G. Ma, and Y. Jing, Observation of degenerate zero-energy topological states at disclinations in an acoustic lattice, Phys. Rev. Lett. **128**, 174301 (2022).
[22] B.-Y. Xie, O. You, and S. Zhang, Photonic topological pump between chiral disclination states, Phys. Rev. A **106**, L021502 (2022).
[23] Z.-K. Lin, Q. Wang, Y. Liu, H. Xue, B. Zhang, Y. Chong, and J.-H. Jiang, Topological phenomena at defects in acoustic, photonic and solid-state lattices, Nat. Rev. Phys. **5**, 483 (2023).
[24] M.-S. Hwang, H.-R. Kim, J. Kim, B.-J. Yang, Y. Kivshar, and H.-G. Park, Vortex nanolaser based on a photonic disclination cavity, Nat. Photonics **18**, 286 (2023).
[25] W. A. Benalcazar, B. A. Bernevig, and T. L. Hughes, Quantized electric multipole insulators, Science **357**, 61 (2017).
[26] B. Bradlyn, L. Elcoro, J. Cano, M. G. Vergniory, Z. Wang, C. Felser, M. I. Aroyo, and B. A. Bernevig, Topological quantum chemistry, Nature (London) **547**, 298 (2017).
[27] C. W. Peterson, T. Li, W. A. Benalcazar, T. L. Hughes, and G. Bahl, A fractional corner anomaly reveals higher-order topology, Science **368**, 1114 (2020).
[28] W. A. Benalcazar, T. Li, and T. L. Hughes, Quantization of fractional corner charge in C_n-symmetric higher-order topological crystalline insulators, Phys. Rev. B **99**, 245151 (2019).
[29] J. Noh, W. A. Benalcazar, S. Huang, M. J. Collins, K. P. Chen, T. L. Hughes, and M. C. Rechtsman, Topological protection of photonic mid-gap defect modes, Nat. Photonics **12**, 408 (2018).
[30] M. Ezawa, Higher-order topological insulators and semimetals on the breathing kagome and pyrochlore lattices, Phys. Rev. Lett. **120**, 026801 (2018).
[31] B.-Y. Xie, H.-F. Wang, H.-X. Wang, X.-Y. Zhu, J.-H. Jiang, M.-H. Lu, and Y.-F. Chen, Second-order photonic topological insulator with corner states, Phys. Rev. B **98**, 205147 (2018).
[32] M. Serra-Garcia, V. Peri, R. Süsstrunk, O. R. Bilal, T. Larsen, L. G. Villanueva, and S. D. Huber, Observation of a phononic quadrupole topological insulator, Nature (London) **555**, 342 (2018).
[33] H. Xue, Y. Yang, F. Gao, Y. Chong, and B. Zhang, Acoustic higher-order topological insulator on a kagome lattice, Nat. Mater. **18**, 108 (2019).
[34] M. Li, D. Zhirihin, M. Gorlach, X. Ni, D. Filonov, A. Slobozhanyuk, A. Alù, and A. B. Khanikaev, Higher-order topological states in photonic kagome crystals with long-range interactions, Nat. Photonics **14**, 89 (2020).
[35] S. Imhof, C. Berger, F. Bayer, J. Brehm, L. W. Molenkamp, T. Kiessling, F. Schindler, C. H. Lee, M. Greiter, T. Neupert, and R. Thomale, Topolectrical-circuit realization of topological corner modes, Nat. Phys. **14**, 925 (2018).
[36] C. M. Bender, Making sense of non-Hermitian Hamiltonians, Rep. Prog. Phys. **70**, 947 (2007).
[37] L. Feng, R. El-Ganainy, and L. Ge, Non-Hermitian photonics based on parity–time symmetry, Nat. Photonics **11**, 752 (2017).
[38] Q. Wang and Y. D. Chong, Non-Hermitian photonic lattices: tutorial, J. Opt. Soc. Am. B **40**, 1443 (2023).
[39] T. E. Lee, Anomalous edge state in a non-Hermitian lattice, Phys. Rev. Lett. **116**, 133903 (2016).
[40] D. Leykam, K. Y. Bliokh, C. Huang, Y. D. Chong, and F. Nori, Edge modes, degeneracies, and topological numbers in non-Hermitian systems, Phys. Rev. Lett. **118**, 040401 (2017).
[41] H. Shen, B. Zhen, and L. Fu, Topological band theory for non-Hermitian Hamiltonians, Phys. Rev. Lett. **120**, 146402 (2018).
[42] Z. Gong, Y. Ashida, K. Kawabata, K. Takasan, S. Higashikawa, and M. Ueda, Topological phases of non-Hermitian systems, Phys. Rev. X **8**, 031079 (2018).
[43] A. Cerjan, S. Huang, M. Wang, K. P. Chen, Y. Chong, and M. C. Rechtsman, Experimental realization of a Weyl exceptional ring, Nat. Photonics **13**, 623 (2019).
[44] A. Ghatak and T. Das, New topological invariants in non-Hermitian systems, J. Phys. Condens. Matter **31**, 263001 (2019).
[45] L. E. F. Torres, Perspective on topological states of non-Hermitian lattices, J. Phys. **3**, 014002 (2019).
[46] K. Kawabata, K. Shiozaki, M. Ueda, and M. Sato, Symmetry and topology in non-Hermitian physics, Phys. Rev. X **9**, 041015 (2019).
[47] M. Parto, Y. G. N. Liu, B. Bahari, M. Khajavikhan, and D. N. Christodoulides, Non-Hermitian and topological photonics: optics at an exceptional point, Nanophotonics **10**, 403 (2021).
[48] E. J. Bergholtz, J. C. Budich, and F. K. Kunst, Exceptional topology of non-Hermitian systems, Rev. Mod. Phys. **93**, 015005 (2021).
[49] F. D. M. Haldane and S. Raghu, Possible realization of directional optical waveguides in photonic crystals with broken time-reversal symmetry, Phys. Rev. Lett. **100**, 013904 (2008).
[50] Z. Wang, Y. Chong, J. D. Joannopoulos, and M. Soljačić, Observation of unidirectional backscattering-immune topological electromagnetic states, Nature (London) **461**, 772 (2009).
[51] L. Lu, J. D. Joannopoulos, and M. Soljačić, Topological photonics, Nat. Photonics **8**, 821 (2014).
[52] Z. Yang, F. Gao, X. Shi, X. Lin, Z. Gao, Y. Chong, and B. Zhang, Topological acoustics, Phys. Rev. Lett. **114**, 114301 (2015).
[53] L. M. Nash, D. Kleckner, A. Read, V. Vitelli, A. M. Turner, and W. T. M. Irvine, Topological mechanics of gyroscopic metamaterials, Proc. Natl. Acad. Sci. U.S.A. **112**, 14495 (2015).
[54] J. Ningyuan, C. Owens, A. Sommer, D. Schuster, and J. Simon, Time- and site-resolved dynamics in a topological circuit, Phys. Rev. X **5**, 021031 (2015).
[55] V. V. Albert, L. I. Glazman, and L. Jiang, Topological properties of linear circuit lattices, Phys. Rev. Lett. **114**, 173902 (2015).
[56] P. St-Jean, V. Goblot, E. Galopin, A. Lemaître, T. Ozawa, L. L. Gratiet, I. Sagnes, J. Bloch, and A. Amo, Lasing in

topological edge states of a one-dimensional lattice, Nat. Photonics **11**, 651 (2017).

[57] M. Parto, S. Wittek, H. Hodaei, G. Harari, M. A. Bandres, J. Ren, M. C. Rechtsman, M. Segev, D. N. Christodoulides, and M. Khajavikhan, Edge-mode lasing in 1d topological active arrays, Phys. Rev. Lett. **120**, 113901 (2018).

[58] M. A. Bandres, S. Wittek, G. Harari, M. Parto, J. Ren, M. Segev, D. N. Christodoulides, and M. Khajavikhan, Topological insulator laser: Experiments, Science **359**, eaar4005 (2018).

[59] Y. Zeng, U. Chattopadhyay, B. Zhu, B. Qiang, J. Li, Y. Jin, L. Li, A. G. Davies, E. H. Linfield, B. Zhang *et al.*, Electrically pumped topological laser with valley edge modes, Nature (London) **578**, 246 (2020).

[60] A. Dikopoltsev, T. H. Harder, E. Lustig, O. A. Egorov, J. Beierlein, A. Wolf, Y. Lumer, M. Emmerling, C. Schneider, S. Höfling, M. Segev, and S. Klembt, Topological insulator vertical-cavity laser array, Science **373**, 1514 (2021).

[61] L. Yang, G. Li, and L. Lu, Topological-cavity surface-emitting laser, Nat. Photonics **16**, 279 (2022).

[62] S. Weimann, M. Kremer, Y. Plotnik, Y. Lumer, S. Nolte, K. G. Makris, M. Segev, M. Rechtsman, and A. Szameit, Topologically protected bound states in photonic parity–time-symmetric crystals, Nat. Mater. **16**, 433 (2017).

[63] K. Kawabata, K. Shiozaki, and M. Ueda, Anomalous helical edge states in a non-Hermitian Chern insulator, Phys. Rev. B **98**, 165148 (2018).

[64] M. Ornigotti and A. Szameit, Quasi PT-symmetry in passive photonic lattices, J. Opt. **16**, 065501 (2014).

[65] K. Takata and M. Notomi, Photonic topological insulating phase induced solely by gain and loss, Phys. Rev. Lett. **121**, 213902 (2018).

[66] S. Liu, S. Ma, C. Yang, L. Zhang, W. Gao, Y. J. Xiang, T. J. Cui, and S. Zhang, Gain- and loss-induced topological insulating phase in a non-Hermitian electrical circuit, Phys. Rev. Appl. **13**, 014047 (2020).

[67] H. Gao, H. Xue, Q. Wang, Z. Gu, T. Liu, J. Zhu, and B. Zhang, Observation of topological edge states induced solely by non-Hermiticity in an acoustic crystal, Phys. Rev. B **101**, 180303(R) (2020).

[68] P. Comaron, V. Shahnazaryan, W. Brzezicki, T. Hyart, and M. Matuszewski, Non-Hermitian topological end-mode lasing in polariton systems, Phys. Rev. Res. **2**, 022051(R) (2020).

[69] X.-W. Luo and C. Zhang, Higher-order topological corner states induced by gain and loss, Phys. Rev. Lett. **123**, 073601 (2019).

[70] H. Gao, H. Xue, Z. Gu, T. Liu, J. Zhu, and B. Zhang, Non-Hermitian route to higher-order topology in an acoustic crystal, Nat. Commun. **12**, 1888 (2021).

[71] Q.-Y. Xu, F. Liu, C.-Z. Chen, and D.-H. Xu, Edge states in a non-Hermitian topological crystalline insulator, Phys. Rev. B **105**, 075411 (2022).

[72] M. L. N. Chen, L. J. Jiang, S. Zhang, R. Zhao, Z. Lan, and W. E. I. Sha, Comparative study of Hermitian and non-Hermitian topological dielectric photonic crystals, Phys. Rev. A **104**, 033501 (2021).

[73] B. Zhu, Q. Wang, Y. Zeng, Q. J. Wang, and Y. D. Chong, Single-mode lasing based on $\mathcal{PT}$-breaking of two-dimensional photonic higher-order topological insulator, Phys. Rev. B **104**, L140306 (2021).

[74] Y. Li, C. Fan, X. Hu, Y. Ao, C. Lu, C. T. Chan, D. M. Kennes, and Q. Gong, Effective Hamiltonian for photonic topological insulator with non-Hermitian domain walls, Phys. Rev. Lett. **129**, 053903 (2022).

[75] F. Schindler and A. Prem, Dislocation non-Hermitian skin effect, Phys. Rev. B **104**, L161106 (2021).

[76] X.-Q. Sun, P. Zhu, and T. L. Hughes, Geometric response and disclination-induced skin effects in non-Hermitian systems, Phys. Rev. Lett. **127**, 066401 (2021).

[77] A. Panigrahi, R. Moessner, and B. Roy, Non-Hermitian dislocation modes: Stability and melting across exceptional points, Phys. Rev. B **106**, L041302 (2022).

[78] B. A. Bhargava, I. C. Fulga, J. van den Brink, and A. G. Moghaddam, Non-Hermitian skin effect of dislocations and its topological origin, Phys. Rev. B **104**, L241402 (2021).

[79] See Supplemental Material, which includes with Refs. [14–16,21,27,38,42,46,65,68,80–87], at http://link.aps.org/supplemental/10.1103/PhysRevLett.133.233804 for discussions on the alternative gain or loss pattern, eigenenergies of the C_4-symmetric disclination lattice, calculation details of the disclination charge, and robustness against disorders, including variations in on-site imaginary potentials and intersite distance-dependent hoppings. Also included is a model for exciton-polaritonic lattices.

[80] T. Jacqmin, I. Carusotto, I. Sagnes, M. Abbarchi, D. D. Solnyshkov, G. Malpuech, E. Galopin, A. Lemaître, J. Bloch, and A. Amo, Direct observation of Dirac cones and a flatband in a honeycomb lattice for polaritons, Phys. Rev. Lett. **112**, 116402 (2014).

[81] M. Wouters and I. Carusotto, Excitations in a nonequilibrium Bose-Einstein condensate of exciton polaritons, Phys. Rev. Lett. **99**, 140402 (2007).

[82] P. Stępnickiand M. Matuszewski, Tight-binding model for exciton-polariton condensates in external potentials, Phys. Rev. A **88**, 033626 (2013).

[83] J. D. Töpfer, I. Chatzopoulos, H. Sigurdsson, T. Cookson, Y. G. Rubo, and P. G. Lagoudakis, Engineering spatial coherence in lattices of polariton condensates, Optica **8**, 106 (2021).

[84] S. Alyatkin, H. Sigurdsson, A. Askitopoulos, J. D. Töpfer, and P. G. Lagoudakis, Quantum fluids of light in all-optical scatterer lattices, Nat. Commun. **12**, 5571 (2021).

[85] A. Baas, J.-P. Karr, M. Romanelli, A. Bramati, and E. Giacobino, Optical bistability in semiconductor microcavities in the nondegenerate parametric oscillation regime: Analogy with the optical parametric oscillator, Phys. Rev. B **70**, 161307(R) (2004).

[86] W. A. Benalcazar and A. Cerjan, Bound states in the continuum of higher-order topological insulators, Phys. Rev. B **101**, 161116(R) (2020).

[87] A. Cerjan, M. Jürgensen, W. A. Benalcazar, S. Mukherjee, and M. C. Rechtsman, Observation of a higher-order topological bound state in the continuum, Phys. Rev. Lett. **125**, 213901 (2020).

[88] L.-H. Wu and X. Hu, Scheme for achieving a topological photonic crystal by using dielectric material, Phys. Rev. Lett. **114**, 223901 (2015).

[89] M. Proctor, P. A. Huidobro, B. Bradlyn, M. B. de Paz, M. G. Vergniory, D. Bercioux, and A. García-Etxarri, Robustness of topological corner modes in photonic crystals, Phys. Rev. Res. **2**, 042038(R) (2020).

[90] M. Blanco de Paz, C. Devescovi, G. Giedke, J. J. Saenz, M. G. Vergniory, B. Bradlyn, D. Bercioux, and A. García-Etxarri, Tutorial: Computing topological invariants in 2d photonic crystals, Adv. Quantum Technol. **3**, 1900117 (2020).

[91] S. J. Palmer and V. Giannini, Berry bands and pseudo-spin of topological photonic phases, Phys. Rev. Res. **3**, L022013 (2021).

[92] J. Ahn, S. Park, D. Kim, Y. Kim, and B.-J. Yang, Stiefel–Whitney classes and topological phases in band theory, Chin. Phys. B **28**, 117101 (2019).

[93] S. Xu, Y. Wang, and R. Agarwal, Absence of topological protection of the interface states in $\mathbb{Z}_2$ photonic crystals, Phys. Rev. Lett. **131**, 053802 (2023).

[94] D. C. Brody, Biorthogonal quantum mechanics, J. Phys. A **47**, 035305 (2013).

[95] F. K. Kunst, E. Edvardsson, J. C. Budich, and E. J. Bergholtz, Biorthogonal bulk-boundary correspondence in non-Hermitian systems, Phys. Rev. Lett. **121**, 026808 (2018).

[96] G.-G. Liu, S. Mandal, P. Zhou, X. Xi, R. Banerjee, Y.-H. Hu, M. Wei, M. Wang, Q. Wang, Z. Gao, H. Chen, Y. Yang, Y. Chong, and B. Zhang, Localization of chiral edge states by the non-Hermitian skin effect, Phys. Rev. Lett. **132**, 113802 (2024).

[97] A. Ghatak, M. Brandenbourger, J. van Wezel, and C. Coulais, Observation of non-Hermitian topology and its bulk–edge correspondence in an active mechanical metamaterial, Proc. Natl. Acad. Sci. U.S.A. **117**, 29561 (2020).

[98] Y. Ota, K. Takata, T. Ozawa, A. Amo, Z. Jia, B. Kante, M. Notomi, Y. Arakawa, and S. Iwamoto, Active topological photonics, Nanophotonics **9**, 547 (2020).

[99] T. Gao, E. Estrecho, K. Y. Bliokh, T. C. H. Liew, M. D. Fraser, S. Brodbeck, M. Kamp, C. Schneider, S. Höfling, Y. Yamamoto, F. Nori, Y. S. Kivshar, A. G. Truscott, R. G. Dall, and E. A. Ostrovskaya, Observation of non-Hermitian degeneracies in a chaotic exciton-polariton billiard, Nature (London) **526**, 554 (2015).

[100] D. Sanvitto and S. Kéna-Cohen, The road towards polaritonic devices, Nat. Mater. **15**, 1061 (2016).

[101] S. Mandal, R. Banerjee, E. A. Ostrovskaya, and T. C. H. Liew, Nonreciprocal transport of exciton polaritons in a non-Hermitian chain, Phys. Rev. Lett. **125**, 123902 (2020).

[102] R. Banerjee *et al.*, Replication Data for: Topological Disclination States and Charge Fractionalization in a Non-Hermitian Lattice (2024), 10.21979/N9/JNAEGE.